Article

Insertion Torque (IT) and Implant Stability Quotient (ISQ) Assessment in Dental Implants with and without Healing Chambers: A Polyurethane In Vitro Study

Bruno Freitas Mello [1], Marcio De Carvalho Formiga [1], Marco Aurélio Bianchini [2], Ivan Borges, Jr. [1], Gustavo Coura [1], Margherita Tumedei [3], Renato Fuller [1], Morena Petrini [4], Tea Romasco [4,5], Paula Vaz [6], Adriano Piattelli [7,8] and Natalia Di Pietro [4,5,*]

[1] Department of Periodontology and Oral Implantology, Unisul University, Florianopolis 88101-001, Brazil; brunofmellofloripa@gmail.com (B.F.M.); marciocformiga@gmail.com (M.D.C.F.); ivan@ivanborgesjr.com.br (I.B.J.); dr.gustavocoura@gmail.com (G.C.); fullerrenato@gmail.com (R.F.)
[2] Post-Graduate Program in Implant Dentistry (PPGO), Federal University of Santa Catarina (UFSC), Florianopolis 88040-900, Brazil; bian07@yahoo.com.br
[3] Department of Medical, Surgical and Dental Sciences, University of Milan, 20122 Milan, Italy; margherita.tumedei@unimi.it
[4] Department of Medical, Oral and Biotechnological Sciences, "G. d'Annunzio" University of Chieti-Pescara, 66013 Chieti, Italy; morena.petrini@unich.it (M.P.); tea.romasco@unich.it (T.R.)
[5] Center for Advanced Studies and Technology-CAST, "G. d'Annunzio" University of Chieti-Pescara, 66013 Chieti, Italy
[6] Fixed Prosthodontics, Genetics-Faculty of Dental Medicine, University of Porto, 4200-393 Porto, Portugal; paula.vaz@gmail.com
[7] School of Dentistry, Saint Camillus International University of Health and Medical Sciences, 00131 Rome, Italy; apiattelli51@gmail.com
[8] Facultad de Medicina, UCAM Universidad Católica San Antonio de Murcia, 30107 Murcia, Spain
[*] Correspondence: natalia.dipietro@unich.it

Abstract: Primary Stability (PS) depends on different factors, such as bone structure (quality and density), implant characteristics (macro and micro), and the relationship between thread shape and implant insertion hole size. PS is crucial for the prognosis and success of dental implants. The use of healing chambers, which create empty spaces between the implant and peri-implant bone, helps reduce the risk of compressive bone necrosis. High Insertion Torque (IT) values could potentially lead to the deterioration of the implant-abutment connection. However, the optimal implant macro-structure and IT values remain unknown. In this study, implants with healing chambers (Test) and without (Control) were inserted into polyurethane blocks with densities of 10, 20, 30, and 40 pounds per cubic foot (PCF). In blocks with densities of 30 and 40 PCF, Control implants had significantly higher IT values than Test implants. Additionally, Control implants exhibited significantly higher Removal Torque (RT) values than Test implants, but only in the 30 PCF density block ($p < 0.0001$). However, no differences were found between the implants in the 10, 20, and 40 PCF density blocks. Similarly, no significant differences were observed in the Implant Stability Quotient (ISQ) values between the Test and Control implants. The results of the present study confirm that adding healing chambers to the macro-structure of dental implants can significantly reduce IT values without affecting ISQ values. This suggests the potential for avoiding compression and damage to peri-implant bone while maintaining consistent levels of PS.

Keywords: dental implants; healing chambers; implant primary stability; insertion torque; polyurethane; removal torque

1. Introduction

One of the most critical prerequisites for achieving mineralized bone at the interface with dental implants is Primary Stability (PS) [1]. This latter depends on various factors,

including bone quality and density, implant micro-geometry, thread shape, and surface characteristics. Equally important is the interaction between the macrostructure of the implant threads and the implant site [1].

Generally, two main strategies aim to achieve mineralized bone at the implant-bone interface. One involves achieving a close adaptation between the implant and bone, especially in underprepared surgical sites. The other strategy creates empty spaces between the implant and the surrounding bone, leading to the formation of the so-called healing chambers [2]. In the first case, very high PS is often achieved through peri-implant bone compression. However, this can potentially lead to bone necrosis and a subsequent decrease in PS in the weeks following implant insertion. High Insertion Torque (IT) values can indeed damage the implant-abutment connection [3]. Nevertheless, the optimal surgical technique, implant macro-geometry, and IT values to achieve maximal bone formation in the peri-implant space, particularly in low-density and low-quality bone, remain unknown [4–6].

The concept of a healing chamber was introduced to mitigate peri-implant bone compression and the potential for bone necrosis [1,2]. This could be attributed to the voids created between the implant's macro-structure and the bone hole site, which are promptly filled with a blood clot following implant insertion. Subsequently, new bone formation occurs through an intra-membranous process [2].

Recent developments have led to the creation of mathematical and biomechanical models for in vitro testing of implant-supported prostheses under various loads [7,8]. Specifically, rigid polyurethane foam, recognized as an isotropic and homogeneous material, has become a standard prototype as per the American Society for Testing and Materials (ASTM F-1839-08 "Standard Specification for Rigid Polyurethane Foam for Use as a Standard Material for Testing Orthopaedic Devices and Instruments") [9]. This foam is employed for testing and demonstrating orthopedic implants, instruments, instrumentation, and for examining force distribution around dental implants in various anatomical locations [10–12]. In particular, the polyurethane foam blocks are designed to closely mimic natural bone density, as classified by Mish based on density, trabecular cortex, and microstructure into four categories: D1, dense cortical bone and poor/absent trabecular bone (mandible symphysis); D2, cortical and dense trabecular bone tissue (mandible and anterior maxilla); D3, thin cortical and trabecular bone (mandible and anterior/posterior maxilla); D4, poor/absent cortical and thin trabecular tissues (posterior maxilla) [13]. Gehrke et al. [4] conducted an in vitro study using polyurethane blocks with low-density rated at 10 and 20 pounds per cubic foot (PCF) to assess the IT, Removal Torque (RT), and Implant Stability Quotient (ISQ) of implants with two different micro-geometries. In all tested groups, implants initially placed in the 10 PCF density blocks exhibited relatively low stability. However, the employment of undersized osteotomies notably increased the measured values in all 20 PCF density blocks. These authors reported that even with a modified (undersized) osteotomy technique, implants inserted into the low-quality bone (Type IV bone) can pose challenges to achieve osseointegration due to their limited initial stability and resistance from the bone. Modifications to the implant macro-geometry, such as the incorporation of healing chambers, resulted in increased bone presence on the implant surface following pullout testing. In 2023, the same authors [14] conducted a clinical study involving 70 patients and 100 implants featuring two different micro-geometries, some with healing chambers and some without. They demonstrated that the implants with healing chambers displayed statistically significant lower IT values and slightly higher ISQ values. In summary, these implants exhibited reduced IT values but slightly higher ISQ values. Dental implants with healing chamber configurations have emerged as a target for improving osseointegration [15].

Considering the aforementioned information, the goal of this study was to investigate the impact of implant healing chambers on IT, RT, and ISQ in an in vitro polyurethane foam model.

2. Materials and Methods

2.1. Dental Implants

The Test titanium implants used in the present in vitro study were Maestro implants (Implacil De Bortoli, Cambuci, São Paulo, Brazil). They were characterized by a conical shape and an internal Cone-Morse abutment joint connection without an anti-rotational index. The head had a straight shape without micro-threads. The body's macro-geometry included groves and healing chambers at the thread profile and apex, designed to enhance blood clot stability and facilitate early bone formation.

The Control titanium implants used were the Due Cone implants (Implacil De Bortoli, Cambuci, São Paulo, Brazil). Similar to the Test implants, they had a conical shape and an internal Cone-Morse abutment joint connection without an anti-rotational index. However, the head had a straight shape without micro-threads or healing chambers.

All implants in the study had a length of 9 mm and a diameter of 4 mm (Figure 1).

Figure 1. Design of the two tested implants: Due Cone (**left**) and Maestro (**right**).

2.2. Experimental Study Design

In the present investigation, a total of 96 implants (48 Test and 48 Control) were included for testing on four polyurethane blocks with varying densities. This configuration provided 24 drilling sites for each block (Figure 2).
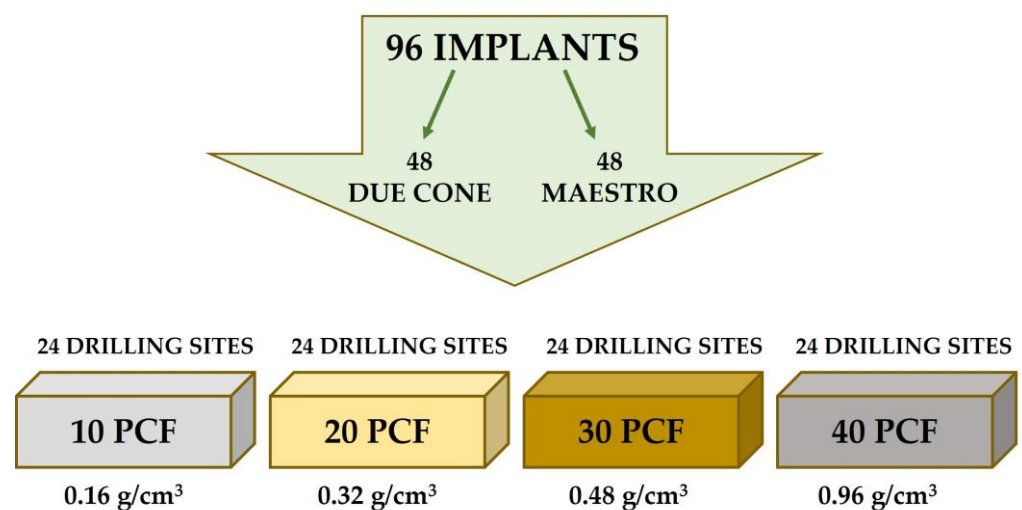
Figure 2. Schematic representation of the in vitro study's experimental design.

2.3. Polyurethane Block Simulator

It has recently been demonstrated that polyurethane exhibits biomechanical properties similar to human bone tissue, including linear elasticity and isotropic constitutive symmetry [10,11,16–18]. These characteristics make polyurethane a suitable material for

conducting biomechanical tests on dental implants, including the assessment of IT, RT, and resonance frequency analysis (RFA) [19]. Furthermore, polyurethane is available in various thicknesses and densities, spanning from D1 to D4, according to Mish classification [13].

The investigation compared the strength values related to IT and RT of Test and Control implants, as well as the ISQ values, when inserted into polyurethane foam blocks of different sizes and densities. To achieve this, the authors selected different types of solid rigid polyurethane foam (Nacional Ossos, São Paulo, Brazil) with consistent dimensions (97 mm × 100 mm × 50 mm) and homogeneous densities. The chosen polyurethane foam densities were 10, 20, 30, and 40 PCF, corresponding to densities of 0.16, 0.32, 0.48, and 0.96 g/cm^3, respectively [19] (Figure 3).

Figure 3. Images of polyurethane foam blocks with different densities: from left to right, 10, 20, 30, and 40 pounds per cubic foot (PCF).

2.4. Implant Drill

The implants were placed following the manufacturer's protocol. Initially, a 2 mm × 10 mm spear drill was used at 900 rpm for the initial milling, followed by a 3.5 mm × 10 mm drill with a staggered pattern at 900 rpm, and finally, a 4 mm × 10 mm drill at 900 rpm, all using a surgical motor (W&H Dentalwerk Bürmoos GmbH, Bürmoos, Austria). Subsequently, the final implant positioning at the bone level was accomplished with a surgical contra-angle handpiece, operating at a calibrated speed of 20 rpm and a torque of 30 Ncm (W&H Dentalwerk Bürmoos GmbH, Bürmoos, Austria) (Figure 4).
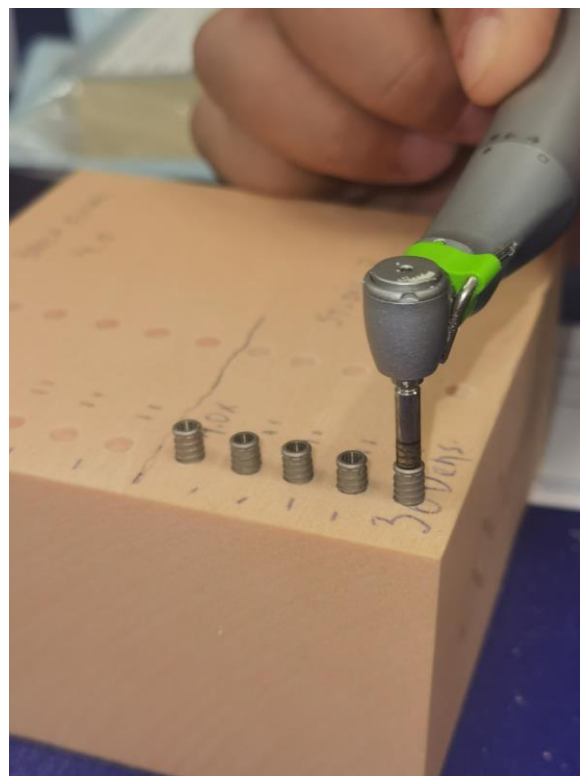
Figure 4. Example of the insertion of a Control implant in a 30 PCF density polyurethane foam block.

2.5. Insertion Torque (IT) and Removal Torque (RT)

While PS is desirable during implant placement, it is the absence of micromotion that ensures predictable implant osseointegration. The use of an increased IT helps achieve PS by minimizing implant micromotion [20]. Overall, IT values (measured in Ncm) represent the force required for the maximum clockwise movement that removed the material.

On the other hand, RT is clinically defined as the force needed to remove the implant from the bone, and it provides a reliable means of assessing PS. In fact, it indirectly provides insights into the extent of bone-to-implant contact (BIC) [21].

IT and RT measurements were obtained using a calibrated torque meter with a range of 5 to 80 Ncm (UNIKA, Oralplant Suisse, Mendrisio, Switzerland). The values were recorded at the final bone level positioning using an advanced force and torque indicator (AFTI, Mecmesin, Slinfold, West Sussex, UK) (Figure 5). The torque values were processed using a specialized electronic database within the ImpDat Plus software package v. 3.95 (East Lansing, MI, USA) installed on a digital card.

Figure 5. Image of the advanced force and torque indicator (AFTI) used to evaluate the insertion torque (IT) and removal torque (RT) values.

2.6. Resonance Frequency Analysis (RFA)

The RFA is a vital parameter for assessing the ISQ after implant placement. This non-invasive technique is valuable for gauging the risk of implant failure and provides additional information about the predictability of dental implant procedures [22].

Consequently, following implant insertion, dental implant PS was determined by calculating ISQ using hand-screwed Smart-Pegs (Osstell Mentor Device, Integration Diagnostic AB, Savadelen, Sweden) placed in the abutment-joint chamber. ISQ values ranged from 0 to 100 (measured between 3500 and 85,000 Hz) and were categorized as low (less than 60 ISQ), medium (60–70 ISQ), and high stability (more than 70 ISQ). Two RFA measurements were taken for each specimen, with measurements performed at two different orientations separated by a 90° angle (Bucco-Lingual: BL and Mesio-Distal: MD), and the average ISQ value was computed (Figure 6).

Figure 6. Example of the implant stability quotient (ISQ) values assessment through a hand-screwed Smart-Pegs.

2.7. Calculation of the Sample Size

G*Power 3.1.9.7 program (Heinrich Heine Universität Düsseldorf, Düsseldorf, Germany) was used to perform the sample size and the power analysis for this study, using the analysis of variance (ANOVA): fixed effects, special, main effects, and interactions statistical test. Considering 4 testing conditions and 2 groups of implants, the following parameters were calculated: effect size: 0.4, α err: 0.05; power (1-β): 0.9; numerator df: 3; the number of groups: 8. The minimum required sample size for statistically significant results was determined to be 93. Therefore, a total of 96 implant sites were included in this study.

2.8. Statistical Analysis

IT, RT, and RFA values, along with intergroup differences, were analyzed using a Two-Way ANOVA test, followed by Tukey's post-hoc test, with statistical significance set at $p < 0.05$. Statistical analysis was conducted with GraphPad 9.0 statistical software package (Prism, San Diego, CA, USA). Descriptive statistics were presented as the mean $\pm$ Standard Deviation (SD).

3. Results

3.1. IT Values

The IT values of Due Cone implants were significantly higher than those of Maestro implants in 30 PCF (27.40 $\pm$ 0.89 Ncm and 19.30 $\pm$ 5.4 Ncm, respectively, with a $p < 0.05$) and 40 PCF (52.60 $\pm$ 4.34 Ncm and 37.20 $\pm$ 3.35 Ncm, respectively, with a $p < 0.0001$) density blocks. Conversely, no statistically significant differences were observed in 10 and 20 PCF density blocks between the two implant types. The lowest IT values were recorded in the 10 PCF density block for both implants (1.00 $\pm$ 0.01 and 0.50 $\pm$ 0.01 Ncm for Due Cone and Maestro implants, respectively), resulting in significantly lower than all other density blocks ($p < 0.0001$). The highest IT values were detected in the 40 PCF density block for Due Cone implants (52.60 $\pm$ 4.34 Ncm) and the 20 PCF density block for Maestro implants (41.20 $\pm$ 3.83 Ncm), resulting in significantly different with a $p < 0.001$. The highest Due Cone implants' IT values significantly surpassed values reported in the 10, 20, and 30 PCF density blocks ($p < 0.0001$, $p < 0.05$, and $p < 0.0001$, respectively), while those of Maestro implants only with respect to 10 and 30 PCF density blocks ($p < 0.0001$). However, the IT values registered for Maestro implants in the 20 PCF density block did not display a significant difference compared to IT values in the 40 PCF density block (41.20 $\pm$ 3.83 Ncm and 37.20 $\pm$ 3.35 Ncm, respectively). A statistically significant difference was also found between 20 and 30 PCF density blocks for both implants (45.60 $\pm$ 3.85 Ncm and 27.40 $\pm$ 0.89 Ncm, respectively, with a $p < 0.0001$ for Due Cone implants; 41.20 $\pm$ 3.83 Ncm and 19.30 $\pm$ 5.43 Ncm, respectively, with a $p < 0.0001$ for Maestro implants) (Figure 7). Confidence Intervals (CI) and *p*-values for each intergroup comparison are provided in Table 1.
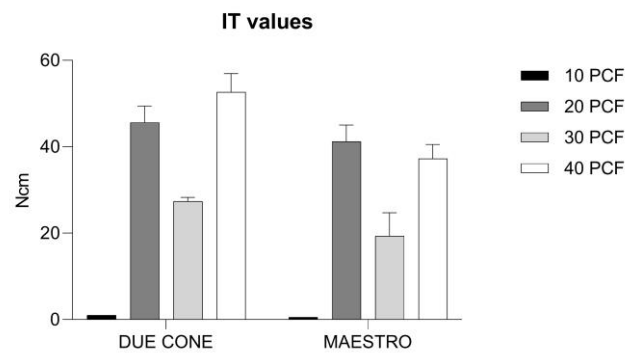
Figure 7. Bar graph reporting IT values of Due Cone and Maestro implants across all polyurethane foam densities.

Table 1. Summary of Insertion Torque (IT) multiple comparisons among all experimental groups. Due Cone implants inserted in (A) 10 pounds per cubic foot (PCF), (B) 20 PCF, (C) 30 PCF, (D) and 40 PCF density blocks compared to Maestro implants in (E) 10 PCF, (F) 20 PCF, (G) 30 PCF, (H) and 40 PCF density blocks. CI: Confidence Interval; ns: not significant.

Tukey's Multiple Comparisons Test	95.00% CI of Difference	Adjusted *p*-Value	Summary
A–B	−51.46 to −37.74	<0.0001	****
A–C	−33.26 to −19.54	<0.0001	****
A–D	−58.46 to −44.74	<0.0001	****
A–E	−6.362 to 7.362	>0.9999	ns
A–F	−47.06 to −33.34	<0.0001	****
A–G	−25.16 to −11.44	<0.0001	****
A–H	−43.06 to −29.34	<0.0001	****
B–C	11.34 to 25.06	<0.0001	****
B–D	−13.86 to −0.1380	0.0429	*
B–E	38.24 to 51.96	<0.0001	****
B–F	−2.462 to 11.26	0.4500	ns
B–G	19.44 to 33.16	<0.0001	****
B–H	1.538 to 15.26	0.0082	**
C–D	−32.06 to −18.34	<0.0001	****
C–E	20.04 to 33.76	<0.0001	****
C–F	−20.66 to −6.938	<0.0001	****
C–G	1.238 to 14.96	0.0118	*
C–H	−16.66 to −2.938	0.0014	**
D–E	45.24 to 58.96	<0.0001	****
D–F	4.538 to 18.26	0.0002	***
D–G	26.44 to 40.16	<0.0001	****
D–H	8.538 to 22.26	<0.0001	****
E–F	−47.56 to −33.84	<0.0001	****
E–G	−25.66 to −11.94	<0.0001	****
E–H	−43.56 to −29.84	<0.0001	****
F–G	15.04 to 28.76	<0.0001	****
F–H	−2.862 to 10.86	0.5683	ns
G–H	−24.76 to −11.04	<0.0001	****

* $p < 0.05$; ** $p < 0.01$; *** $p < 0.001$; **** $p < 0.0001$.

3.2. RT Values

RT values for Due Cone implants were significantly higher than those for Maestro implants only in the 30 PCF density block (2.74 ± 0.05 Ncm and 1.90 ± 0.26 Ncm, respectively, with a $p < 0.0001$). No differences were observed between the two implants in the 10, 20, and 40 PCF density blocks. Significantly higher RT values were found for both Due Cone and Maestro implants when comparing the 10 PCF density block to the other blocks ($p < 0.0001$ for Due Cone implants; $p < 0.0001$ vs. 20 and 40 PCF density blocks, and $p < 0.05$ vs. 30 PCF density block for Maestro implants). Additionally, both implants displayed the highest RT values in the 40 PCF density block (3.94 ± 0.05 Ncm for Due Cone implants and 3.70 ± 0.28 Ncm for Maestro implants), which were significantly higher compared to values registered for the same implants in 20 and 30 PCF density blocks ($p < 0.01$ and $p < 0.0001$, respectively, for Due Cone implants; $p < 0.0001$ for Maestro implants). Contrarily, both

implants expressed the lowest RT values in the 10 PCF density block (1.28 ± 0.08 Ncm for Due Cone implants and 1.44 ± 0.33 Ncm for Maestro implants). Moreover, significantly higher RT values were observed in the 20 PCF density block compared to the 30 PCF density block for both implants (3.36 ± 0.26 Ncm and 2.74 ± 0.05 Ncm, respectively, with a $p < 0.0001$ for Due Cone implants; 3.00 ± 0.19 Ncm and 1.90 ± 0.26 Ncm, respectively, with a $p < 0.0001$ for Maestro implants) (Figure 8). In Table 2, Confidence Intervals and p-values have been reported for each intergroup comparison.
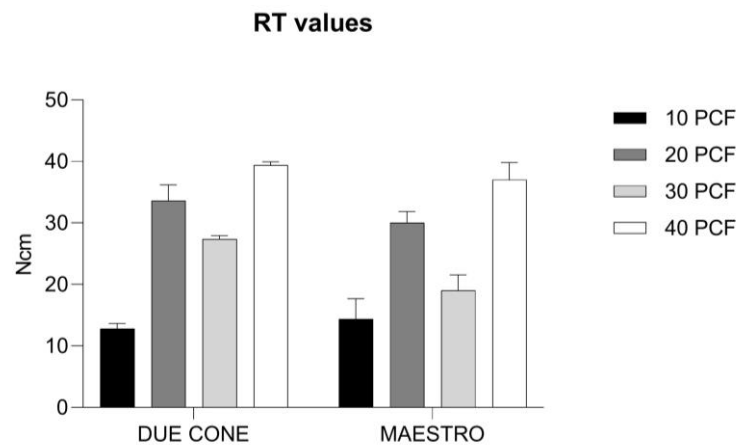
Figure 8. Bar graph reporting RT values of Due Cone and Maestro implants across all polyurethane foam densities.

Table 2. Summary of Removal Torque (RT) multiple comparisons among all experimental groups.

Tukey's Multiple Comparisons Test	95.00% CI of Difference	Adjusted p-Value	Summary
A–B	−25.20 to −16.40	<0.0001	****
A–C	−19.00 to −10.20	<0.0001	****
A–D	−31.00 to −22.20	<0.0001	****
A–E	−6.000 to 2.800	0.9324	ns
A–F	−21.60 to −12.80	<0.0001	****
A–G	−10.60 to −1.800	0.0016	**
A–H	−28.60 to −19.80	<0.0001	****
B–C	1.800 to 10.60	0.0016	**
B–D	−10.20 to −1.400	0.0036	**
B–E	14.80 to 23.60	<0.0001	****
B–F	−0.8000 to 8.000	0.1754	ns
B–G	10.20 to 19.00	<0.0001	****
B–H	−7.800 to 1.000	0.2304	ns
C–D	−16.40 to −7.600	<0.0001	****
C–E	8.600 to 17.40	<0.0001	****
C–F	−7.000 to 1.800	0.5517	ns
C–G	4.000 to 12.80	<0.0001	****
C–H	−14.00 to −5.200	<0.0001	****
D–E	20.60 to 29.40	<0.0001	****
D–F	5.000 to 13.80	<0.0001	****
D–G	16.00 to 24.80	<0.0001	****
D–H	−2.000 to 6.800	0.6455	ns
E–F	−20.00 to −11.20	<0.0001	****
E–G	−9.000 to −0.2000	0.0353	*
E–H	−27.00 to −18.20	<0.0001	****
F–G	6.600 to 15.40	<0.0001	****
F–H	−11.40 to −2.600	0.0003	***
G–H	−22.40 to −13.60	<0.0001	****

$*$ $p < 0.05$; $**$ $p < 0.01$; $***$ $p < 0.001$; $****$ $p < 0.0001$.

3.3. RFA Values

No differences were observed in ISQ values when comparing Due Cone and Maestro implants in each polyurethane bone density.

However, both implants displayed significantly higher ISQ values ($p < 0.0001$) when inserted into the 40 PCF density block compared to the 10 PCF density block in both orientations. Particularly, in the BL orientation the ISQ values were 75.20 ± 1.10 ISQ for Due Cone implants and 75.00 ± 0.71 ISQ for Maestro implants in the 40 PCF density block, while 51.80 ± 1.79 ISQ for Due Cone implants and 56.00 ± 7.97 ISQ for Maestro implants in the 10 PCF density block. In the MD orientation, instead, the ISQ values were 74.80 ± 1.92 ISQ for Due Cone implants and 74.40 ± 0.89 ISQ for Maestro implants in the 40 PCF density block, while 40.60 ± 3.29 ISQ for Due Cone implants and 49.00 ± 11.51 ISQ for Maestro implants in the 10 PCF density block.

Contrarily, no differences were found when comparing the highest values to those of the same implants inserted into 20 and 30 PCF density blocks. Specifically, in the BL orientation Due Cone implants expressed 69.60 ± 2.30 ISQ and 71.00 ± 0.71 ISQ, respectively, while Maestro implants were 68.60 ± 2.07 ISQ and 69.20 ± 4.97 ISQ, respectively. In the MD orientation Due Cone implants expressed 70.60 ± 0.89 ISQ and 6.20 ± 4.44 ISQ, respectively, while Maestro implants were 69.40 ± 1.95 ISQ and 65.40 ± 2.97 ISQ, respectively.

The lowest RFA values were recorded in the lowest-density block of 10 PCF for both implants. For Due Cone implants they were 51.80 ± 1.79 ISQ in the BL orientation and 40.60 ± 3.29 ISQ in the MD orientation. Instead, for Maestro implants they were 56.00 ± 8.00 ISQ in the BL orientation and 49.00 ± 11.51 ISQ in the MD orientation. These values were significantly lower if compared to all the other blocks. Indeed, in the BL orientation, they expressed a $p < 0.0001$ if compared to 20 (69.60 ± 2.30 ISQ), 30 (71.00 ± 0.71 ISQ), and 40 (75.20 ± 1.10 ISQ) PCF density blocks for Due Cone implants, while a $p < 0.001$ if compared to the 20 PCF density block (68.60 ± 2.07 ISQ) and a $p < 0.0001$ compared to 30 (69.20 ± 4.97 ISQ) and 40 (75.00 ± 0.71 ISQ) PCF density blocks for Maestro implants. As regards the MD orientation, they expressed a $p < 0.0001$ if compared to 20 (70.60 ± 0.89 ISQ), 30 (67.20 ± 4.44 ISQ), and 40 (74.40 ± 0.89 ISQ) PCF density blocks for Due Cone implants, while a $p < 0.001$ if compared to the 30 PCF density block (65.40 ± 2.97 ISQ) and a $p < 0.0001$ compared to 20 (69.40 ± 1.95 ISQ) and 40 (74.40 ± 0.89 ISQ) PCF density blocks for Maestro implants (Figure 9). Table 3 provided Confidence Intervals and *p*-values for each intergroup comparison.
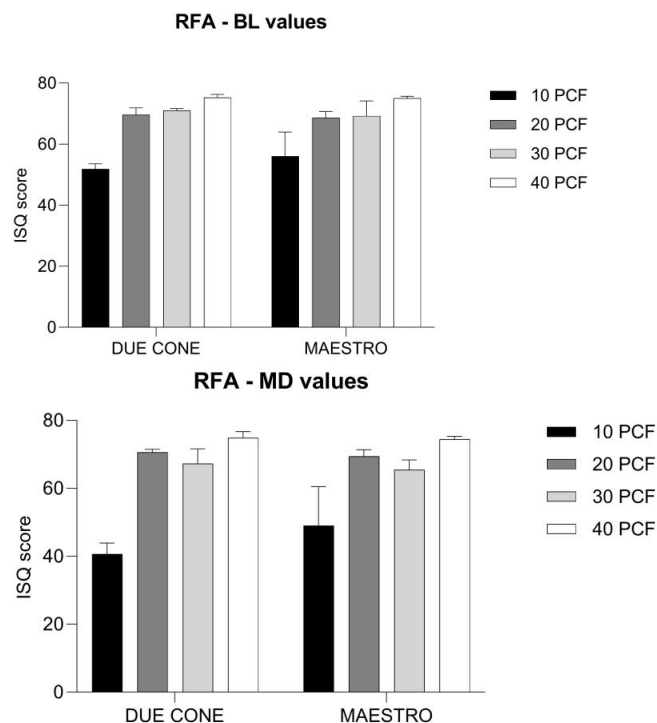
Figure 9. Bar graphs reporting Resonance Frequency Analysis (RFA) values recorded in Bucco-Lingual (RFA-BL) and Mesio-Distal (RFA-MD) orientations. Values were expressed in the ISQ score and measured after the insertion of Due Cone and Maestro implants in all polyurethane foam densities.

Table 3. Summary of Resonance Frequency Analysis (RFA) multiple comparisons among all experimental groups. RFA-BL: Resonance Frequency Analysis measured in the Bucco-Lingual orientation; RFA-MD: Resonance Frequency Analysis measured in the Mesio-Distal orientation.

RFA-BL			
Tukey's Multiple Comparisons Test	**95.00% CI of Difference**	**Adjusted *p*-Value**	**Summary**
A–B	−25.16 to −10.44	<0.0001	****
A–C	−26.56 to −11.84	<0.0001	****
A–D	−30.76 to −16.04	<0.0001	****
A–E	−11.56 to 3.158	0.5934	ns
A–F	−24.16 to −9.442	<0.0001	****
A–G	−24.76 to −10.04	<0.0001	****
A–H	−30.56 to −15.84	<0.0001	****
B–C	−8.758 to 5.958	0.9984	ns
B–D	−12.96 to 1.758	0.2463	ns
B–E	6.242 to 20.96	<0.0001	****
B–F	−6.358 to 8.358	0.9998	ns
B–G	−6.958 to 7.758	>0.9999	ns
B–H	−12.76 to 1.958	0.2862	ns
C–D	−11.56 to 3.158	0.5934	ns
C–E	7.642 to 22.36	<0.0001	****
C–F	−4.958 to 9.758	0.9612	ns
C–G	−5.558 to 9.158	0.9924	ns
C–H	−11.36 to 3.358	0.6493	ns
D–E	11.84 to 26.56	<0.0001	****
D–F	−0.7583 to 13.96	0.1049	ns
D–G	−1.358 to 13.36	0.1785	ns
D–H	−7.158 to 7.558	>0.9999	ns
E–F	−19.96 to −5.242	0.0001	***
E–G	−20.56 to −5.842	<0.0001	****
E–H	−26.36 to −11.64	<0.0001	****
F–G	−7.958 to 6.758	>0.9999	ns
F–H	−13.76 to 0.9583	0.1260	ns
G–H	−13.16 to 1.558	0.2104	ns
RFA-MD			
Tukey's multiple comparisons test	**95.00% CI of difference**	**Adjusted *p*-value**	**Summary**
A–B	−39.74 to −20.26	<0.0001	****
A–C	−36.34 to −16.86	<0.0001	****
A–D	−43.94 to −24.46	<0.0001	****
A–E	−18.14 to 1.342	0.1324	ns
A–F	−38.54 to −19.06	<0.0001	****
A–G	−34.54 to −15.06	<0.0001	****
A–H	−43.54 to −24.06	<0.0001	****
B–C	−6.342 to 13.14	0.9450	ns
B–D	−13.94 to 5.542	0.8522	ns
B–E	11.86 to 31.34	<0.0001	****
B–F	−8.542 to 10.94	>0.9999	ns
B–G	−4.542 to 14.94	0.6692	ns
B–H	−13.54 to 5.942	0.9054	ns
C–D	−17.34 to 2.142	0.2207	ns
C–E	8.458 to 27.94	<0.0001	****
C–F	−11.94 to 7.542	0.9953	ns
C–G	−7.942 to 11.54	0.9987	ns
C–H	−16.94 to 2.542	0.2783	ns
D–E	16.06 to 35.54	<0.0001	****
D–F	−4.342 to 15.14	0.6274	ns
D–G	−0.3422 to 19.14	0.0649	ns
D–H	−9.342 to 10.14	>0.9999	ns
E–F	−30.14 to −10.66	<0.0001	****
E–G	−26.14 to −6.658	0.0001	***
E–H	−35.14 to −15.66	<0.0001	****
F–G	−5.742 to 13.74	0.8805	ns
F–H	−14.74 to 4.742	0.7100	ns
G–H	−18.74 to 0.7422	0.0871	ns

*** $p < 0.001$; **** $p < 0.0001$.

4. Discussion

Usually, forces of 30 Ncm or higher are commonly employed for implant placement in healed ridges or fresh extraction sockets, particularly when immediate implant loading is planned. Higher IT ($\geq$50 Ncm) has the advantage of reducing micromotion without causing any damage to the surrounding bone [20].

The primary finding of this study highlights the significant role of the implant healing chamber profile in reducing IT and RT peaks, particularly in very high-density artificial bone (exceeding 30 PCF in density). This observation is crucial for preventing excessive stress at the peri-implant bone shoulder and minimizing bone remodeling during the early healing phases, especially in D1/D2 bone densities, according to the Misch classification [13]. Beyond its biological advantages, the reduction in torque can help prevent mechanical stress and structural failures of the prosthetic joint, including fixture damage and implant body fractures, which are considered major sources of complications [23,24]. Similarly, no statistically significant differences in PS were observed between Test and Control implants when the polyurethane density was below 30 PCF. The 10 PCF density block, comparable to the D4 bone type [13], presented the most challenging PS scenario for both implant micro-geometries. Specifically, this simulation test was conducted without a cortical bone layer, emulating a full-density bone block with potential translational issues concerning surgical anatomy.

Several studies in the literature support the beneficial effects of implant healing chambers on bone formation and stability. Buser et al. [25] found increased new bone formation in minipigs using implants with two circular bone chambers. Coelho et al. [2] observed rapid filling of healing chambers with woven bone in a dog study. Marin et al. [26] reported woven osseous tissue formation in healing chambers during the initial healing period in another animal study. Similar findings were reported by Bonfante et al. [27] and Baires-Campos et al. [28] in dog studies. Additionally, other studies noted that apically located implant chambers positively influenced bone formation and that trapezoidal chamber configurations enhanced BIC percentage [29,30]. Furthermore, it was also demonstrated that larger osteotomies, generated through osseodensification, induce the formation of healing chambers at the implant-bone interface without affecting PS. In a sheep study, Parra et al. [31] found vertical chambers between threads resulting in close contact between implant and bone. Therefore, these chambers create favorable conditions for blood clot stability and osteogenesis, providing a virtual space for bone-implant interaction.

In this regard, Gehrke et al. [32] analyzed the effect of four different implant macro-geometries on early bone formation in an animal model. Among the three types of implants studied—cylindrical-conical, tapered, and tapered implants with healing chambers- higher values of ISQ, BIC, and other histological parameters were observed when compared to cylindrical implants. Additionally, the same authors reported that implants with healing chambers, despite exhibiting lower IT values, demonstrated reduced vertical bone loss compared to implants with higher IT values. This finding highlights that the presence of healing chambers significantly enhances the bone tissue response [15,33].

The existing literature also includes in vitro studies that employed polyurethane with varying cortical thicknesses. These studies found that incorporating healing chambers into an implant's macro-geometry led to reductions in IT values, while no significant effect on ISQ values was reported [1].

Furthermore, it has been reported that the utilization of implants with healing chambers significantly enhances the progression of peri-implant bone formation [34]. Achieving an appropriate balance between tensile and compressive forces exerted on the peri-implant bone is crucial, and the incorporation of healing chambers could contribute to achieving this balance [35]. Coelho et al. [2] reported that the healing process following implant insertion into the bone site is primarily influenced by the implant's macro-structure and the dimensions of the bone cavity in which the implants are placed. According to these authors, an implant design that includes healing chambers demonstrates greater efficacy in promoting early bone healing. Similar findings were also presented by Gehrke et al. [34], who proved that the utilization of healing chambers enhances and expedites the osseointegration process.

Moreover, the outcomes of this in vitro research are corroborated by earlier in vivo studies. These studies demonstrated how these implant design characteristics contribute to lowering IT values, resulting in reduced peri-implant bone compression, while simultaneously promoting the generation of new bone, new vessels, and a cellular pre-osteogenic matrix [34]. Importantly, these design features do not influence the dimension of the bone osteotomy or the ISQ, despite the decrease in IT values [1].

Regarding the limitations of the present study, it is crucial to acknowledge that although rigid polyurethane foam blocks are already employed in implant research due to their consistent and replicable testing properties, serving as an alternative test material to human cadaver and animal bones, they are unable to fully replicate the intricate characteristics of real bone. To facilitate a more comprehensive discussion of the data, several factors require consideration, including the absence of individual human variability, the natural responses of real bone, and the intricate microenvironment of both healthy and pathological bone conditions. Additionally, it is essential to factor in variables associated with the surgical techniques applied, as a more nuanced understanding of these findings hinges upon such considerations. Consequently, it is worth noting that the data acquired from this study might not perfectly mirror the true in vivo performance of the implants being investigated.

Nevertheless, obtaining crucial corroboration of this data through both animal and clinical studies remains essential for its future application and implementation. To further enhance the utilization of polyurethane blocks as a human bone model for studying implant behavior, including stress and local deformations on the implant-material contact points, particularly within healing chambers, it could be advantageous to conduct biomechanical evaluations through Finite Element Analysis (FEA) studies.

Despite the limitations inherent in conducting in vitro studies on non-human bone tissue, the authors can speculate that these preliminary results offer valuable insights into the biomechanical behavior of these implants. This, in turn, aims to assist clinicians in refining their surgical planning and predicting the prognosis of the dental implant procedure.

5. Conclusions

The current data not only confirmed previously reported findings but also supported the thesis that incorporating healing chambers into the dental implant's structural composition could lead to a substantial reduction in IT values while maintaining unaffected ISQ levels. In conclusion, this approach could result in a reduced risk of peri-implant bone compression damage, along with a notable improvement in expediting the osseointegration process, all while preserving high levels of implant PS.

References

1. Gehrke, S.A.; Pérez-Díaz, L.; Mazón, P.; De Aza, P.N. Biomechanical Effects of a New Macrogeometry Design of Dental Implants: An In Vitro Experimental Analysis. *J. Funct. Biomater.* **2019**, *10*, 47. [CrossRef] [PubMed]
2. Coelho, P.G.; Suzuki, M.; Marin, C.; Granato, R.; Gil, L.F.; Tovar, N.; Jimbo, R.; Neiva, R.; Bonfante, E.A. Osseointegration of Plateau Root Form Implants: Unique Healing Pathway Leading to Haversian-Like Long-Term Morphology. *Adv. Exp. Med. Biol.* **2015**, *881*, 111–128. [CrossRef] [PubMed]
3. Gehrke, S.A.; Pereira, G.M.A.; Gehrke, A.F.; Junior, N.D.B.; Dedavid, B.A. Effects of Insertion Torque on the Structure of Dental Implants with Different Connections: Experimental Pilot Study in Vitro. *PLoS ONE* **2021**, *16*, e0251904. [CrossRef]
4. Gehrke, S.A.; Scarano, A.; de Lima, J.H.C.; Bianchini, M.A.; Dedavid, B.A.; De Aza, P.N. Effects of the Healing Chambers in Implant Macrogeometry Design in a Low-Density Bone Using Conventional and Undersized Drilling. *J. Int. Soc. Prev. Commun. Dent.* **2021**, *11*, 437–447. [CrossRef] [PubMed]
5. Scarano, A.; Carinci, F.; Lorusso, F.; Festa, F.; Bevilacqua, L.; Santos de Oliveira, P.; Maglione, M. Ultrasonic vs Drill Implant Site Preparation: Post-Operative Pain Measurement through VAS, Swelling and Crestal Bone Remodeling: A Randomized Clinical Study. *Materials* **2018**, *11*, 2516. [CrossRef]
6. Maglione, M.; Bevilacqua, L.; Dotto, F.; Costantinides, F.; Lorusso, F.; Scarano, A. Observational Study on the Preparation of the Implant Site with Piezosurgery vs. Drill: Comparison between the Two Methods in Terms of Postoperative Pain, Surgical Times, and Operational Advantages. *BioMed Res. Int.* **2019**, *2019*, 8483658. [CrossRef]
7. Romanos, G.E.; Delgado-Ruiz, R.A.; Sacks, D.; Calvo-Guirado, J.L. Influence of the implant diameter and bone quality on the primary stability of porous tantalum trabecular metal dental implants: An in vitro biomechanical study. *Clin. Oral Implant. Res.* **2018**, *6*, 649–655. [CrossRef]
8. Cipollina, A.; Ceddia, M.; Di Pietro, N.; Inchingolo, F.; Tumedei, M.; Romasco, T.; Piattelli, A.; Specchiulli, A.; Trentadue, B. Finite Element Analysis (FEA) of a Premaxillary Device: A New Type of Subperiosteal Implant to Treat Severe Atrophy of the Maxilla. *Biomimetics* **2023**, *8*, 336. [CrossRef]
9. *ASTM F1839*; Standard Specification for Rigid Polyurethane Foam for Use as a Standard Material for Testing Orthopaedic Devices and Instruments. American Society for Testing and Materials (ASTM): West Conshohocken, PA, USA, 2008. [CrossRef]
10. Di Stefano, D.A.; Arosio, P.; Gastaldi, G.; Gherlone, E. The insertion torque-depth curve integral as a measure of implant primary stability: An in vitro study on polyurethane foam blocks. *J. Prosthet. Dent.* **2018**, *5*, 706–714. [CrossRef]
11. Tsolaki, I.N.; Tonsekar, P.P.; Najafi, B.; Drew, H.J.; Sullivan, A.J.; Petrov, S.D. Comparison of osteotome and conventional drilling techniques for primary implant stability: An in vitro study. *J. Oral Implant.* **2016**, *42*, 321–325. [CrossRef]
12. Comuzzi, L.; Tumedei, M.; Di Pietro, N.; Romasco, T.; Heydari Sheikh Hossein, H.; Montesani, L.; Inchingolo, F.; Piattelli, A.; Covani, U. A Comparison of Conical and Cylindrical Implants Inserted in an In Vitro Post-Extraction Model Using Low-Density Polyurethane Foam Blocks. *Materials* **2023**, *16*, 5064. [CrossRef] [PubMed]
13. Misch, C.E. *Bone Density: A Key Determinant for Treatment Planning. Contemporary Implant Dentistry*, 3rd ed.; Mosby: St. Louis, MO, USA, 2007; pp. 130–146.
14. Gehrke, S.A.; Cortellari, G.C.; De Oliveira Fernandes, G.V.; Scarano, A.; Martins, R.G.; Cançado, R.M.; Mesquita, A.M.M. Randomized Clinical Trial Comparing Insertion Torque and Implant Stability of Two Different Implant Macrogeometries in the Initial Periods of Osseointegration. *Medicina* **2023**, *59*, 168. [CrossRef] [PubMed]
15. Gehrke, S.A.; Eliers Treichel, T.L.; Pérez-Díaz, L.; Calvo-Guirado, J.L.; Aramburú Júnior, J.; Mazón, P.; De Aza, P.N. Impact of Different Titanium Implant Thread Designs on Bone Healing: A Biomechanical and Histometric Study with an Animal Model. *J. Clin. Med.* **2019**, *8*, 777. [CrossRef]
16. Calvert, K.L.; Trumble, K.P.; Webster, T.J.; Kirkpatrick, L.A. Characterization of commercial rigi d polyurethane foams used as bone analogs for implant testing. *J. Mater. Sci. Mater. Med.* **2010**, *21*, 1453–1461. [CrossRef]
17. Nagaraja, S.; Palepu, V. Comparisons of Anterior Plate Screw Pullout Strength Between Polyurethane Foams and Thoracolum-bar Cadaveric Vertebrae. *J. Biomech. Eng.* **2016**, *138*, 104505. [CrossRef] [PubMed]
18. Al-Tarawneh, S.; Thalji, G.; Cooper, L. Macrogeometric Differentiation of Dental Implant Primary Stability: An In Vitro Study. *Int. J. Oral Maxillofac. Implant.* **2022**, *37*, 1110–1118. [CrossRef] [PubMed]
19. Comuzzi, L.; Tumedei, M.; Covani, U.; Romasco, T.; Petrini, M.; Montesani, L.; Piattelli, A.; Di Pietro, N. Primary Stability Assessment of Conical Implants in Under-Prepared Sites: An In Vitro Study in Low-Density Polyurethane Foams. *Appl. Sci.* **2023**, *13*, 6041. [CrossRef]
20. Greenstein, G.; Cavallaro, J. Implant Insertion Torque: Its Role in Achieving Primary Stability of Restorable Dental Implants. *Compend. Contin. Educ. Dent.* **2017**, *38*, 88–96.
21. Simeone, S.G.; Rios, M.; Simonpietri, J. "Reverse torque of 30 Ncm applied to dental implants as test for osseointegration"—Ahuman observational study. *Int. J. Implant. Dent.* **2016**, *2*, 26. [CrossRef]
22. Meredith, N.; Alleyne, D.; Cawley, P. Quantitative determination of the stability of the implant-tissue interface using resonance-frequency analysis. *Clin. Oral Implant. Res.* **1996**, *7*, 261–267. [CrossRef]
23. Gil, F.J.; Herrero-Climent, M.; Lázaro, P.; Rios, J.V. Implant–Abutment Connections: Influence of the Design on the Microgap and Their Fatigue and Fracture Behavior of Dental Implants. *J. Mater. Sci. Mater. Med.* **2014**, *25*, 1825–1830. [CrossRef] [PubMed]
24. Gahlert, M.; Burtscher, D.; Grunert, I.; Kniha, H.; Steinhauser, E. Failure Analysis of Fractured Dental Zirconia Implants. *Clin. Oral Implant. Res.* **2012**, *23*, 287–293. [CrossRef] [PubMed]

25. Buser, D.; Broggini, N.; Wieland, M.; Schenk, R.K.; Denzer, A.J.; Cochran, D.L.; Hoffmann, B.; Lussi, A.; Steinemann, S.G. Enhanced Bone Apposition to a Chemically Modified SLA Titanium Surface. *J. Dent. Res.* **2004**, *83*, 529–533. [CrossRef]

26. Marin, C.; Granato, R.; Suzuki, M.; Gil, J.N.; Janal, M.N.; Coelho, P.G. Histomorphologic and Histomorphometric Evaluation of Various Endosseous Implant Healing Chamber Configurations at Early Implantation Times: A Study in Dogs: Healing of Various Healing Chambers Configurations. *Clin. Oral Implant. Res.* **2010**, *21*, 577–583. [CrossRef] [PubMed]

27. Bonfante, E.A.; Granato, R.; Marin, C.; Suzuki, M.; Oliveira, S.R.; Giro, G.; Coelho, P.G. Early Bone Healing and Biomechanical Fixation of Dual Acid-Etched and as-Machined Implants with Healing Chambers: An Experimental Study in Dogs. *Int. J. Oral Maxillofac. Implant.* **2011**, *26*, 75–82.

28. Baires-Campos, F.-E.; Jimbo, R.; Bonfante, E.-A.; Fonseca-Oliveira, M.-T.; Moura, C.; Zanetta-Barbosa, D.; Coelho, P.-G. Drilling Dimension Effects in Early Stages of Osseointegration and Implant Stability in a Canine Model. *Med. Oral* **2015**, *20*, e471–e479. [CrossRef] [PubMed]

29. Meirelles, L.; Brånemark, P.-I.; Albrektsson, T.; Feng, C.; Johansson, C. Histological Evaluation of Bone Formation Adjacent to Dental Implants with a Novel Apical Chamber Design: Preliminary Data in the Rabbit Model: Novel Apical Chamber Design. *Clin. Implant. Dent. Relat. Res.* **2015**, *17*, 453–460. [CrossRef]

30. Beutel, B.G.; Danna, N.R.; Granato, R.; Bonfante, E.A.; Marin, C.; Tovar, N.; Suzuki, M.; Coelho, P.G. Implant Design and Its Effects on Osseointegration over Time within Cortical and Trabecular Bone. *J. Biomed. Mater. Res.* **2016**, *104*, 1091–1097. [CrossRef]

31. Parra, M.; Benalcázar Jalkh, E.B.; Tovar, N.; Torroni, A.; Badalov, R.M.; Bonfante, E.A.; Nayak, V.; Castellano, A.; Coelho, P.G.; Witek, L. The Influence of Surface Treatment on Osseointegration of Endosteal Implants Presenting Decompressing Vertical Chambers: An In Vivo Study in Sheep. *Int. J. Oral Maxillofac. Implant.* **2022**, *37*, 929–936. [CrossRef]

32. Gehrke, S.A.; Júnior, J.A.; Eirles Treichel, T.L.; Dedavid, B.A. Biomechanical and Histological Evaluation of Four Different Implant Macrogeometries in the Early Osseointegration Process: An in Vivo Animal Study. *J. Mech. Behav. Biomed. Mater.* **2022**, *125*, 104935. [CrossRef]

33. Gehrke, S.A.; Júnior, J.A.; Treichel, T.L.E.; do Prado, T.D.; Dedavid, B.A.; de Aza, P.N. Effects of Insertion Torque Values on the Marginal Bone Loss of Dental Implants Installed in Sheep Mandibles. *Sci. Rep.* **2022**, *12*, 538. [CrossRef] [PubMed]

34. Gehrke, S.A.; Aramburú, J.; Pérez-Díaz, L.; Do Prado, T.D.; Dedavid, B.A.; Mazon, P.; De Aza, P.N. Can Changes in Implant Macrogeometry Accelerate the Osseointegration Process?: An in Vivo Experimental Biomechanical and Histological Evaluations. *PLoS ONE* **2020**, *15*, e0233304. [CrossRef] [PubMed]

35. Gehrke, S.A.; Aramburú Júnior, J.; Pérez-Díaz, L.; Treichel, T.L.E.; Dedavid, B.A.; De Aza, P.N.; Prados-Frutos, J.C. New Implant Macrogeometry to Improve and Accelerate the Osseointegration: An In Vivo Experimental Study. *Appl. Sci.* **2019**, *9*, 3181. [CrossRef]